Progress In Electromagnetics Research M, Vol. 92, 21–30, 2020

Circularly Polarized Single Feed Hemispherical Dielectric Resonator Antenna for Wi-Max Applications

Arunodayam R. Anu[1, *], Parambil Abdulla[1], Puthenveetil M. Jasmine[2], and Thulaseedharan K. Rekha[3]

Abstract—A concentric circular slots coupled hemispherical dielectric resonator antenna fed by a modified microstrip line for circular polarization is investigated. By adjusting the position of the hemispherical dielectric resonator antenna and the slots properly, the resonances of the slot and the antenna are merged to obtain wider axial ratio bandwidth. Parametric studies have been done on the effect of changing the DRA position on impedance band and axial ratio band. The circular polarization achieved by the antenna offers a very good 10 dB impedance bandwidth of 27.379% and a 3 dB axial ratio bandwidth of 640 MHz. The maximum gain in the operational band is 7.3 dBi. The antenna is suitable for Wi-Max applications.

1. INTRODUCTION

Dielectric resonator antennas (DRAs) have received tremendous attention from researchers over the past three decades. DRAs have numerous attractive features such as design flexibility, wide bandwidth, high radiation efficiency, low conductor loss, ease of excitation, and small size. DRA acquires wider impedance bandwidth than microstrip patch antenna because the whole DRA surface acts as an efficient radiator except the ground part, whereas only two narrow radiation sides act as a radiator for microstrip patch antenna [1]. For a long time, studies on DRAs have been concentrated on linear polarization. Circular polarization (CP) is useful in wireless (e.g., mobile and Wi-MAX) and satellite communications due to the insensitivity to transmitter and receiver orientations, effective coverage area, weather penetration, and reduced multipath reflection [2]. A number of excitation methods like coaxial probe, direct microstrip, aperture coupled microstrip, waveguide, coplanar waveguide, etc. have been applied to DRAs [3–6]. Among different excitation schemes, aperture coupled microstrip feed line is most commonly used as it enables direct integration with a printed feed structure and avoids spurious radiation from the feed network. In 1985, Haneishi & Takazava presented the first circularly polarized DRA, using geometrical variation in DRA [7]. A complicated DRA structure with a simple feed excitation has been presented in [8] which produces CP fields when two opposite corners of the DRA are removed at 45°. However, deformation in the DRA shape is difficult to achieve. Oliver et al. [9] and Esselle [10] obtained CP DRA by using a conventional rectangular DRA, with the coupling slot inclined at 45°. A rectangular slot coupled dielectric resonator antenna array making 45° with the slot is also used to produce CP [11]. A CP cylindrical DRA array integrated with helical exciter is proposed in [12]. Single probe feeds are used to obtain CP DRAs [13]. Split ring resonators inside a slot antenna are rotated and fed by a microstrip open-loop feed to produce CP [14]. CP DRA for handheld RFID reader is obtained in [15]. However, the axial ratio bandwidth obtained is small in all cases.

Received 24 February 2020, Accepted 24 April 2020, Scheduled 4 May 2020
* Corresponding author: Arunodayam Radhakrishnan Anu (aranu17@gmail.com).
[1] School of Engineering, Cochin University of Science and Technology, Kochi 22, Kerala, India. [2] MES College, Marampally, Kerala, India. [3] NSS College, Rajakumari, Kerala, India.

Several designs of circularly polarized DRAs employing multiple and single feed methods have been introduced in the literature. A complicated feed structure like a quadrature strip-fed method is used to excite a pair of degenerate modes in a dual/wide-band CP cylindrical DRA [16]. In many CP DRA designs, frequency mismatching occurs between impedance bandwidth and axial ratio bandwidth. In [17], an aperture-coupled stair-shaped DRA with a wide impedance bandwidth of 36.6% but having only a 3-dB axial ratio bandwidth (ARBW) of 11% is implemented.

It is still a challenge to obtain wide impedance and axial ratio bandwidth simultaneously for designing a wideband and good performing CP DRA. Single-feed or multiple-feed configuration can be used to obtain circular polarization. The single-feed configurations are simple and require less space on the feed substrate. The feed losses in the single-feed configuration are less than those in multiple-feed configurations. A single feed circularly polarized DRA has less complexity and is desirable in situations where it is difficult to place dual orthogonal feeds. In this structure, a hemispherical dielectric resonator antenna (HDRA) is excited by three concentric circular slots etched in the ground plane of an FR4 substrate with a modified microstrip line on the other side. CP is obtained by accurately positioning three rings. The three slot rings together with the modified microstrip line offer good coupling and bandwidth improvement between the microstrip line and HDRA.

2. ANTENNA CONFIGURATION

Figure 1(a) shows the geometry of the suggested circularly polarized concentric ring aperture coupled HDRA. The dielectric resonator is made of alumina material (Al_2O_3) having permittivity $\varepsilon_r = 9.8$. The HDRA of radius 12.7 mm is located at an offset position $a_y = 11$ mm along the positive Y direction and

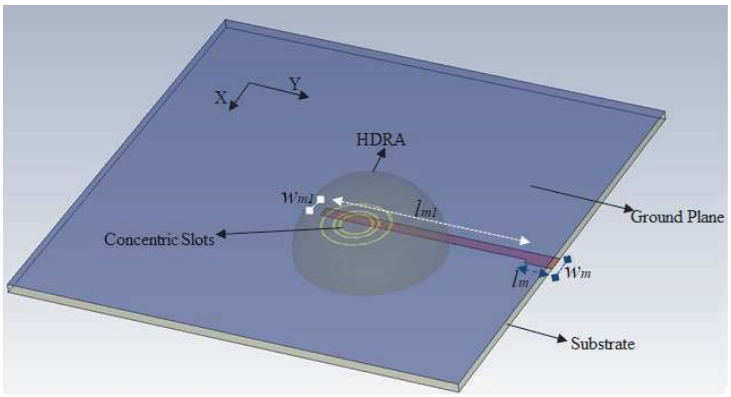

(a)

(b)

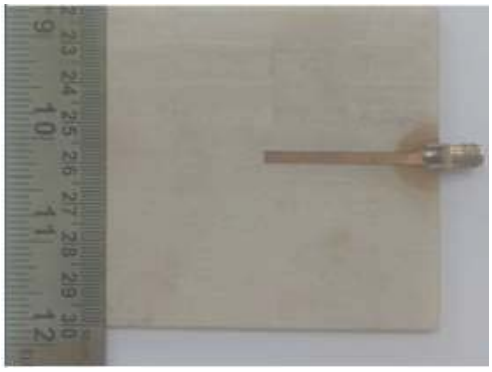

(c)

Figure 1. (a) Configuration of the proposed CP HDRA. (b) Top view of prototype antenna. (c) Bottom view of prototype antenna.

an offset position $a_x = 18\,\text{mm}$ along the positive X direction in the ground plane. An FR4 substrate with a thickness of 1.6 mm, length and width of 80 mm × 80 mm is used as the ground plane. The HDRA is excited by three concentric ring slots etched on the ground plane of the dielectric substrate. The centers of the ring-shaped slots are at (6 mm, −6 mm, 1.6 mm). The innermost slot has an inner radius of 2.5 mm and width 0.5 mm. The middle slot has an inner radius of 3.5 mm and width 0.5 mm. The inner radius of the outermost slot is 5.55 mm and width 0.45 mm. The feed line is composed of a 50 Ω input impedance microstrip line and a stub line etched on the other side of the substrate. The microstrip line has length $lm1 = 5\,\text{mm}$, width $Wm1 = 3\,\text{mm}$, and the stub line is continued after the microstrip line which has length $lm = 36.7\,\text{mm}$ and width $Wm = 2.85\,\text{mm}$. The top and bottom views of the fabricated structure are shown in Figure 1(b) and Figure 1(c).

The HDRA of radius 12.7 mm based on the above material specification will resonate at 3.5 GHz with TE_{111} being the dominant mode when given an appropriate feed. The design of a simple HDRA geometry is given as below.

$$f_r = \frac{4.775 \times 10^7 \text{Re}\,(\text{k}_a)}{(\varepsilon_r)\,a} \tag{1}$$

where 'f_r' is the resonant frequency, 'ε_r' the dielectric constant of the HDRA, 'a' the radius of the hemisphere, and 'k_a' the wavenumber in the dielectric [18].

The slots are accurately positioned so that two near-degenerate orthogonal modes of equal amplitude and 90° phase quadrature are excited at frequencies close to the dominant TE_{111} mode of the HDRA. By adjusting the DRA position with respect to the slot, the resonances of the slot and the DRA can be merged to obtain wider axial ratio bandwidth. The resonant frequency of the slot away from that of the DRA is brought near the DRA resonance by proper excitation of the two orthogonal modes. The electric field distribution observed inside the HDRA and the slots at different phases, 0°, 90°, 180°, and 270° are shown in Figure 2. The circularly polarized field of the proposed antenna has been confirmed by the rotation of E-field in the HDRA. It is observed that the electric field lines take

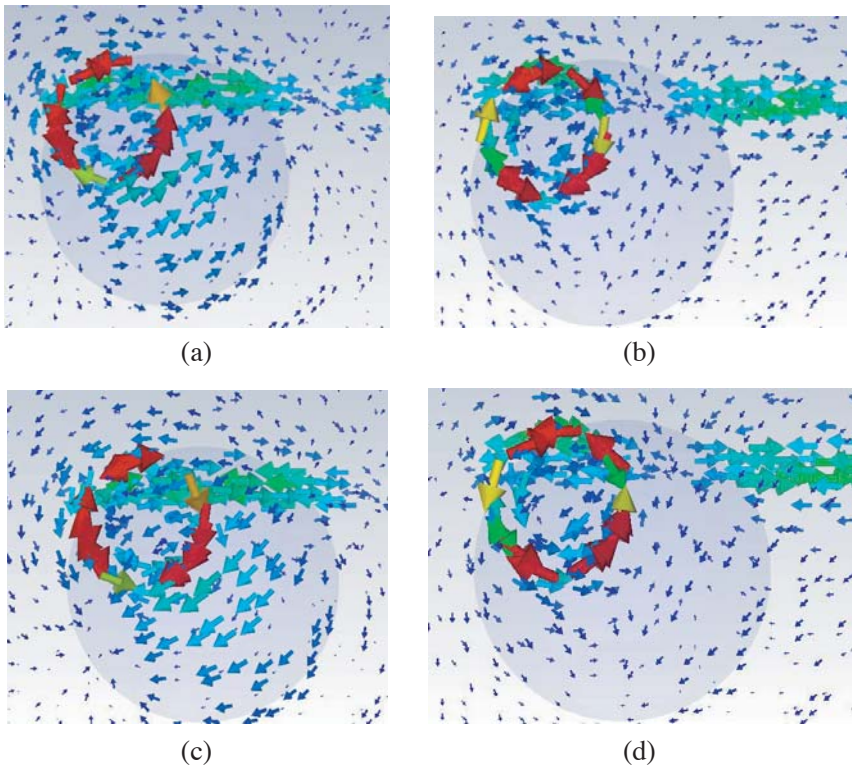

Figure 2. Simulated electric field distribution at four different phase angles, (a) 0°, (b) 90°, (c) 180°, (d) 270° at 3.31 GHz.

a complete rotation in fundamental mode TE_{111}. At phase angle $\phi = 0°$, electric field lines are equal in magnitude and opposite in direction to that at $\phi = 180°$, and the same is the case when $\phi = 90°$ and $\phi = 270°$. It is observed from Figure 2 that if the phase is shifted from 0° to 90° the rotation of E-field inside the HDRA is also shifted from right to left and confirms the formation of orthogonal modes. The electric field vector undergoes rotation with an advance in phase. Rotation is observable in both clockwise and counter-clockwise directions explaining the presence of both right-handed circular polarization (RHCP) and left-handed circular polarization (LHCP). The direction of rotation of the electric field vector is clockwise as the direction of view chosen is from $+Z$-axis, and the sense of polarization is confirmed as RHCP. The direction of rotation of the vector is counter-clockwise as the direction of view chosen is from the $-Z$-axis, and the sense of polarization is confirmed as LHCP.

3. PARAMETRIC ANALYSIS

The parametric analysis has been carried out by CST microwave studio for proper tuning of degenerative modes. The position of the DRA with respect to the slot, which is responsible for circular polarization, is varied along X and Y directions with respect to the ground plane. The effect of changing the DRA position on impedance bandwidth and 3 dB axial ratio bandwidth are studied to detect the amount of coupling and circular polarization. The number of concentric circular slots was chosen based on the parametric study conducted on the dimension of the circular slots. Detailed analysis shows that on adding three slots one by one, the impedance bandwidth as well as axial ratio bandwidth can be improved.

3.1. Deviation of DRA Offset along X Direction (a_x)

The position of the DRA with respect to the three concentric slots along X direction is varied from 17.6 mm to 18.4 mm keeping other factors fixed. Figure 3(a) shows that as the offset value of the DRA with respect to the slot is increased along X direction from 17.6 mm to 18.4 mm, the 10 dB impedance band is shifted towards right. Similarly, Figure 3(b) shows the change in the axial ratio as the position of the DRA with respect to the slot is increased from 17.6 mm to 18.4 mm. From the plot, it can be analyzed that at an offset of 18 mm, there is good control of the axial ratio, and the ARBW obtained is 660 MHz, 18.75% (3.19 GHz–3.85 GHz). The change in offset along the X direction can control the axial ratio and the shift in the 10 dB impedance bandwidth.

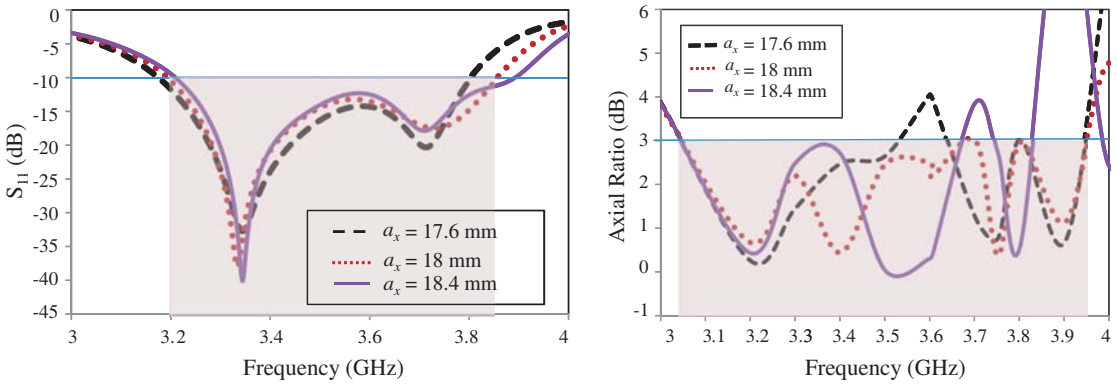

Figure 3. Parametric analysis by varying the DRA offset along with x-direction. (a) S_{11}. (b) Axial Ratio.

3.2. Deviation of DRA Offset along Y Direction (a_y)

The position of the DRA with respect to the three concentric slots along Y direction is varied from 10.6 mm to 11.4 mm keeping other factors fixed. Figure 4(a) shows that as the offset value of the

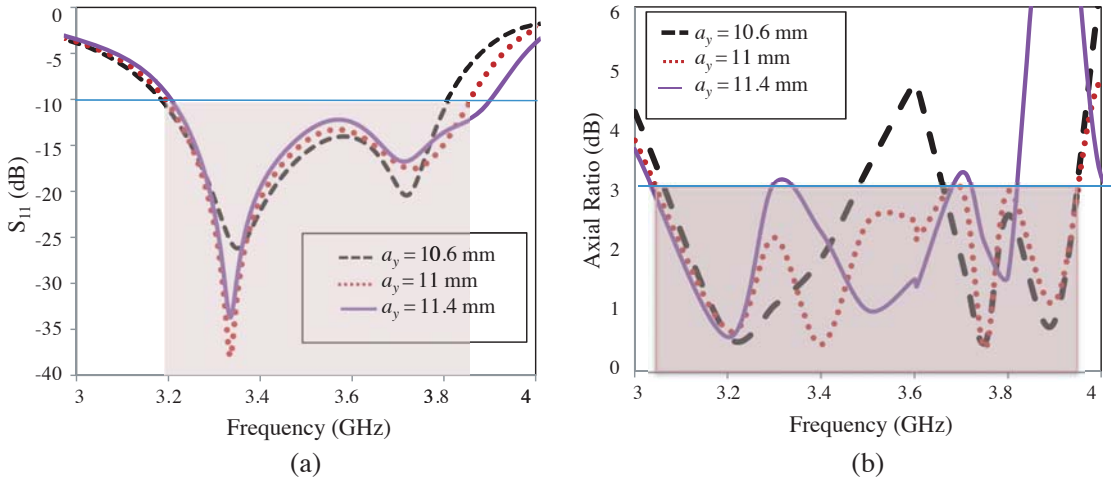

Figure 4. Parametric analysis by varying the DRA offset along y-direction. (a) S_{11}. (b) Axial Ratio.

DRA with respect to the slot is increased along Y direction from 10.6 mm to 11.4 mm, the 10 dB impedance bandwidth is increased from 17.76% (3.18 GHz–3.80 GHz) to 19.71% (3.20 GHz–3.90 GHz). Also, Figure 4(b) shows that the axial ratio bandwidth can be controlled as the position of the DRA with respect to the slot is increased from 10.6 mm to 11.4 mm. The maximum ARBW of 660 MHz, 18.75% (3.19 GHz–3.85 GHz) is obtained at an offset value of 11 mm. Thus we can conclude that the change in the offset value along X as well as Y direction has good control over the 10 dB impedance bandwidth as well as the ARBW.

3.3. Effect of Concentric Slots on DRA

The parametric studies on the slot width of a single circular slot (outer slot) on DRA, having inner radius 5.55 mm and outer radius 6 mm, are carried out where the inner radius of the slot remains the same, but the outer radius is parametrically changed from 5.9 mm to 6.1 mm, and the corresponding plots on return loss and axial ratio are depicted in Figure 5 and Figure 6.

In Figure 5, dual bands are obtained. As the outer radius value (slot width) is increased, the 2nd band shifts towards higher frequency. The axial ratio shows two peaks at 3.5 and 3.7 GHz in Figure 6. To improve the axial ratio bandwidth, these peaks need to be reduced. It is seen that at outer radius 5.9 mm, the axial ratio bandwidth is less than other two outer radii if the peak at 3.5 and 3.7 GHz is reduced. On the contrary, the peak value at 3.7 GHz is less at 6 mm than at 6.1 mm outer radius. Fixing 6 mm as the outer radius shows more chances to improve the axial ratio bandwidth.

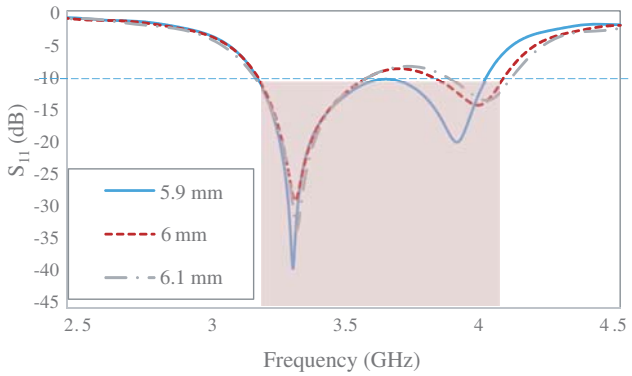

Figure 5. S_{11} plot of variation on slot width of DRA excited by outer slot alone.

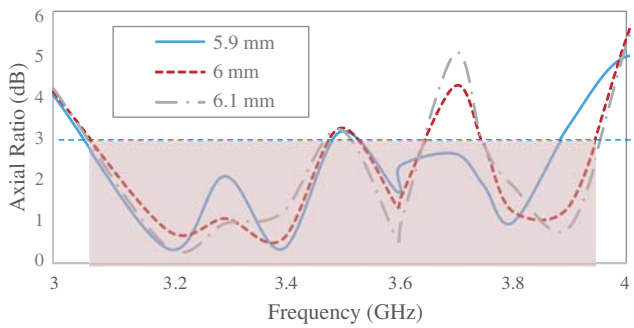

Figure 6. Axial ratio plot of variation on slot width of DRA excited by outer slot alone.

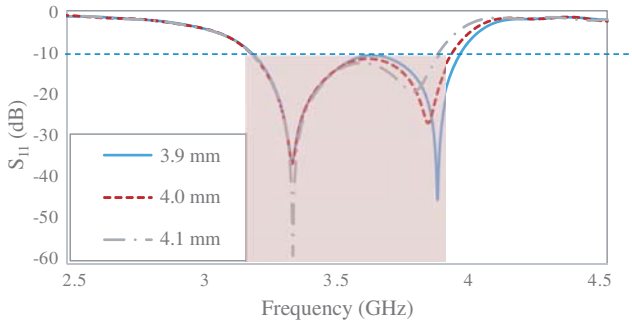

Figure 7. S_{11} plot of variation on slot width of middle slot fixing outer slot value constant.

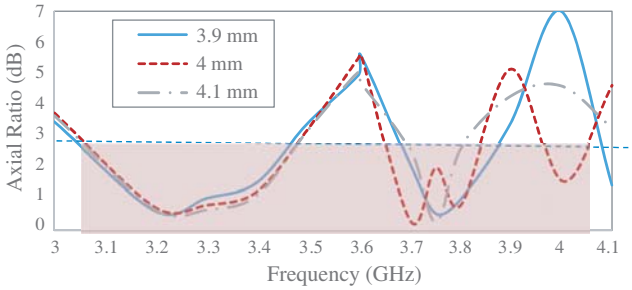

Figure 8. Axial Ratio of variation on slot width of middle slot fixing outer slot value constant.

To enhance the impedance bandwidth and axial ratio bandwidth, one more slot (middle slot) is included inside the former slot, having inner radius fixed at 3.5 mm and the outer radius parametrically changed from 3.9 mm to 4.1 mm, and its corresponding return loss and axial ratio plots are as shown in Figure 7 and Figure 8. There is an increase in the impedance bandwidth, but the axial ratio again shows two peaks at 3.6 GHz and at frequencies after 3.8 GHz. Henceforth, the value 4 mm is chosen as it shows more chances to improve the axial ratio bandwidth within the impedance bandwidth.

Again, in order to enhance the impedance bandwidth and axial ratio bandwidth further, one more slot inside the first slot and second slot is included, having inner radius fixed at 2.5 mm and the outer radius parametrically changed from 2.9 mm to 3.1 mm, and its return loss and axial ratio plots are shown in Figure 9 and Figure 10. There is an increase in the impedance bandwidth as well as axial ratio bandwidth. Henceforth, the value 3 mm is chosen as it shows more improvement towards obtaining the maximum axial ratio bandwidth within the impedance bandwidth.

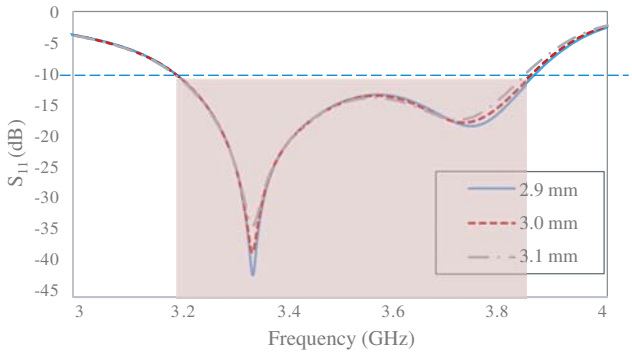

Figure 9. S_{11} plot of variation on slot width of inner slot fixing both outer and middle slot value constant.

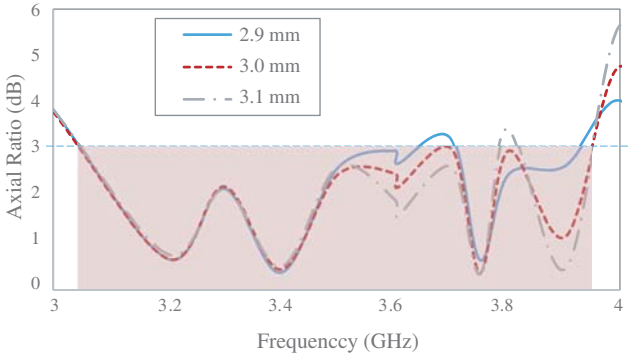

Figure 10. Axial Ratio of variation on slot width of inner slot fixing both outer and middle slot value constant.

4. RESULTS AND DISCUSSION

The proposed antenna is designed and simulated using CST microwave studio. The input reflection coefficient is measured by Rohde & Schwarz ZVL 13 Vector Network Analyzer. The measured and simulated S_{11} are compared as shown in Figure 11. Two resonant frequencies can be found in the measured S_{11} curve. The lower resonant frequency (about 3.55 GHz) and the higher one (about 4.24 GHz) are due to the resonance of the slot. Both the DRA and slot resonances are shifted from their free resonance values. The resonance depicted in the figure indicates that this resonance is due to the merging of resonances of the DRA and slot. The measured 10 dB impedance bandwidth is 27.379% (3.31 GHz–4.36 GHz), and the simulated 10 dB impedance bandwidth is 18.75% (3.19 GHz–3.85 GHz).

The measured response shows an upward shift of 120 MHz with respect to the simulated response due to some fabrication errors that include roughness of the DRA and ground plane surfaces forming air gaps between them [19]. The simulated and measured axial ratios are compared as shown in Figure 12. The simulated axial ratio bandwidth is 18.75% (3.19 GHz–3.85 GHz), and the measured axial ratio

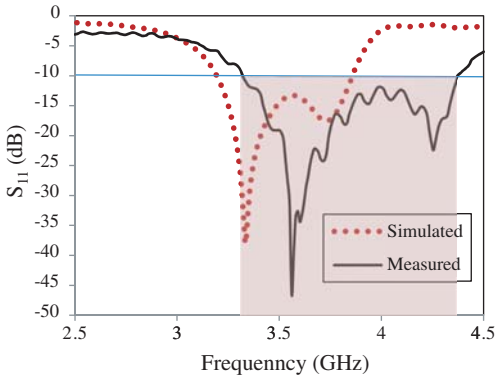

Figure 11. Simulated and measured S_{11} of the proposed antenna.

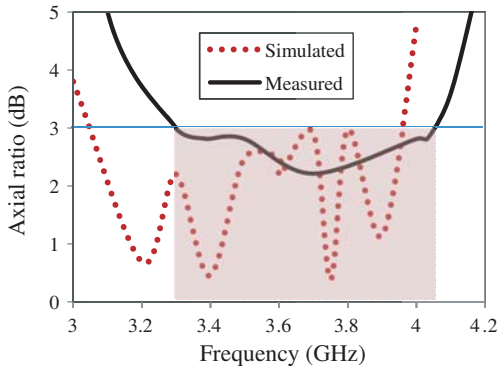

Figure 12. Simulated and measured Axial Ratio plot of the proposed antenna.

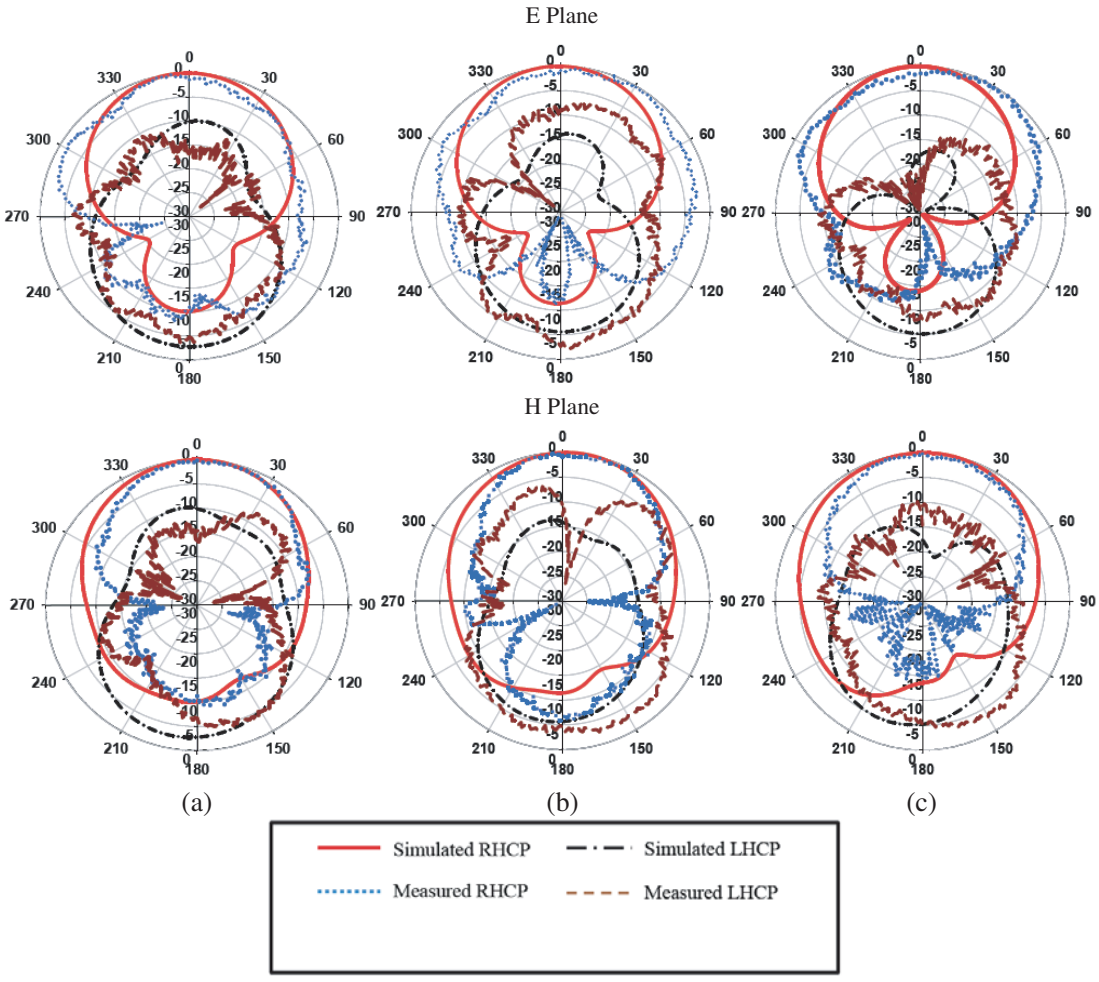

Figure 13. Simulated and measured radiation patterns of proposed antenna at (a) 3.4 GHz, (b) 3.5 GHz, (c) 3.84 GHz.

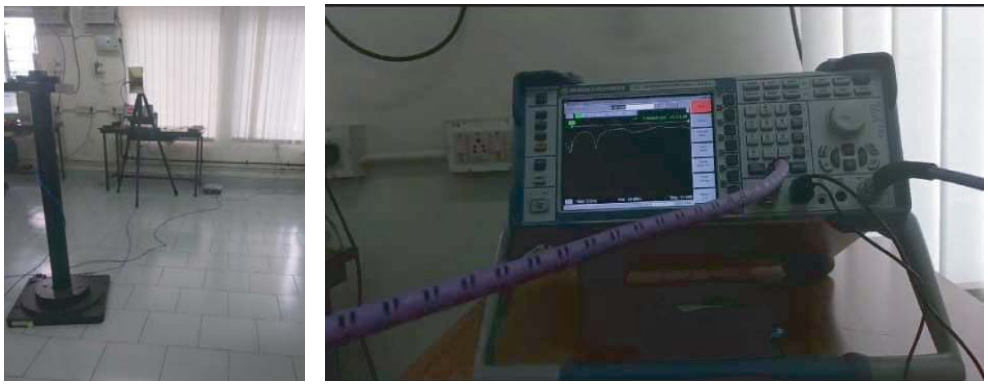

(a) (b)

Figure 14. (a) The radiation pattern measurement setup. (b) Input reflection coefficient measured by Rohde & Schwarz ZVL 13 Vector Network Analyzer.

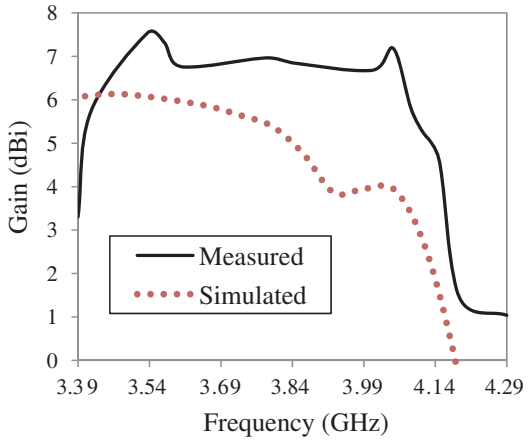

Figure 15. Simulated and Measured gain of the proposed antenna.

Table 1. Comparison of Axial Ratio Bandwidth to previously published antenna structures.

Circular polarized DRA				
Ref	**Shape of DR**	ε_r	f_o **(GHz)**	**3-dB ARBW (%)**
[20]	Rectangular	**9.8**	3.57	16.5
[21]	Rectangular DRA with inclined slots	**15**	2.4	7.3
[22]	Circular sector DRA	**21**	2.675	10
[23]	Cylindrical DRA	**10.2**	6.75	15.9
[24]	cylindrical DRA with L shaped slot	**6.15**	9.5	10.5
[25]	Slot coupled HDRA with parasitic patch	**9.5**	3.50	3.4
This work	**HDRA**	**9.8**	**3.84**	**17.25**

bandwidth is 17.25% (3.39 GHz–4.03 GHz).

The simulated E-plane and H-plane radiation patterns of the antenna have been calculated at the selected frequencies of 3.4 GHz, 3.5 GHz, and 3.84 GHz. The radiation patterns are also measured in the same selected frequencies. Figure 13 shows the simulated and measured E-plane and H-plane radiation patterns at 3.4 GHz, 3.5 GHz, and 3.84 GHz. The antenna has a broadside radiation pattern.

The radiation pattern measurement setup and the input reflection coefficient measured by Rohde & Schwarz ZVL 13 Vector Network Analyzer are shown in Figure 14(a) and Figure 14(b).

The plot of simulated and measured gains versus frequency are shown in Figure 15. The antenna attains a maximum measured gain of 7.3 dBi in the operational band. Table 1 illustrates the comparison of axial ratio bandwidth to other published works in literature. It is noted that the proposed work shows progress in axial ratio bandwidth within the operational band over prior reported designs.

The 3 dB axial ratio bandwidth of the proposed antenna measured is found to be 640 MHz (3.39 GHz–4.03 GHz, 17.25%) in the broadside direction ($\theta = 0°$, $\phi = 0°$).

5. CONCLUSION

In this structure, a circularly polarized concentric ring slot coupled HDRA has been proposed and experimentally investigated. The DRA is excited by three concentric ring slots etched on the ground plane to generate circular polarization. The circular polarization achieved by the proposed antenna offers a 10 dB impedance bandwidth of 27.379%. The proposed CP HDRA has 3-dB ARBW of 17.25% (3.39 GHz–4.03 GHz) falling within its 10-dB impedance passband making its entire ARBW usable. The maximum gain is 7.3 dBi in the operational band. The proposed antenna can be used for the Wi-MAX application.

ACKNOWLEDGMENT

The authors would like to acknowledge the financial support from the University Grants Commission.

REFERENCES

1. Luk, K. M. and K. W. Leung, *Dielectric Resonator Antennas*, Research Studies, Press Ltd., Hertfordshire, England, UK, 2003.
2. Iwasaki, H., "A circularly polarized small-size microstrip antenna with a cross slot," *IEEE Transactions on Antennas and Propagation*, Vol. 44, No. 10, 1399–1401, 1996.
3. Abdulla, P., A. B. Kakade, Y. K. Singh, and A. Chakrabarty, "Analysis of dielectric resonator antenna excited by a slot at the waveguide shorted end," *Microwave and Optical Technology Letters*, Vol. 50, No. 5, 1356–1359, 2008.
4. Kumar, R., S. R. Thummaluru, and R. K. Chaudhary, "Improvements in Wi-MAX reception: A new dual-mode wideband circularly polarized dielectric resonator antenna," *IEEE Antennas and Propagation Magazine*, Vol. 61, No. 1, 41–49, 2019.
5. Yang, W.-W., W.-J. Sun, H. Tang, and J.-X. Chen, "Design of a circularly polarized dielectric resonator antenna with wide bandwidth and low axial ratio values," *IEEE Transactions on Antennas and Propagation*, Vol. 67, No. 3, 1963–1968, 2019.
6. Altaf, A. and M. Seo, "Dual-band circularly polarized dielectric resonator antenna for WLAN and WiMAX applications," *Sensors*, Vol. 20, No. 4, 1137, 2020.
7. Haneishi, M. and H. Takazawa, "Broadband circularly polarized planar array composed of a pair of dielectric resonator antennas," *Electronics Letters*, Vol. 21, No. 10, 437–438, 1985.
8. Fang, X., K. W. Leung, and E. H. Lim, "Singly-fed dual-band circularly polarized dielectric resonator antenna," *IEEE Antennas and Wireless Propagation Letters*, Vol. 13, 995–998, 2014.
9. Oliver, M. B., Y. M. M. Antar, R. K. Mongia, and A. Ittipiboon, "Circularly polarised rectangular dielectric resonator antenna," *Electronics Letters*, Vol. 31, No. 6, 418–419, 1995.
10. Esselle, K. P., "Circularly polarised higher-order rectangular dielectric-resonator antenna," *Electronics Letters*, Vol. 32, No. 3, 150–151, 1996.
11. Ain, M. F., Y. M. A. Qasaymeh, Z. A. Ahmad, M. A. Zakariya, M. A. Othman, S. S. Olokede, and M. Z. Abdullah, "Novel modeling and design of circularly polarized dielectric resonator antenna array," *Progress In Electromagnetics Research C*, Vol. 28, 165–179, 2012.

12. Rana, B. and S. K. Parui, "High gain circularly-polarized dielectric resonator antenna array with helical exciter," *Progress In Electromagnetics Research Letters*, Vol. 44, 107–111, 2014.
13. Malekabadi, A., M. H. Neshati, and J. Rashed-Mohassel, "Circular polarized dielectric resonator antennas using a single probe feed," *Progress In Electromagnetics Research C*, Vol. 3, 81–94, 2008.
14. Parvathy, A. R., V. G. Ajay, and M. Thomaskutty, "Circularly polarized split ring resonator loaded slot antenna," *Advanced Electromagnetics*, Vol. 7, No. 5, 1–6, 2018.
15. Zainud-Deen, S. H., H. A. Malhat, N. A. El-Shalaby, and K. H. Awadalla, "Dielectric resonator antenna mounted on cylindrical ground plane for handheld RFID reader at 5.8 GHz," *Advanced Electromagnetics*, Vol. 1, No. 3, 1–6, 2018.
16. Fang, X. S. and K. W. Leung, "Linear-/circular-polarization designs of dual-/wide-band cylindrical dielectric resonator antennas," *IEEE Transactions on Antennas and Propagation*, Vol. 60, No. 6, 2662–2671, 2012.
17. Chair, R., S. L. S. Yang, A. A. Kishk, K. F. Lee, and K. M. Luk, "Aperture fed wideband circularly polarized rectangular stair shaped dielectric resonator antenna," *IEEE Transactions on Antennas and Propagation*, Vol. 54, No. 4, 1350–1352, 2006.
18. Mukherjee, B., P. Patel, G. S. Reddy, and J. Mukherjee, "A novel half hemispherical dielectric resonator antenna with array of slots for wideband applications," *Progress In Electromagnetics Research C*, Vol. 36, 207–221, 2013.
19. Muhammed, J. P., A. Parambil, and R. P. Muhammad, "Analysis and experiment of stair-shaped waveguide-fed dielectric resonator antenna," *IET Microwaves, Antennas & Propagation*, Vol. 10, No. 4, 453–458, 2016.
20. Kumar, R. and R. K. Chaudhary, "Modified microstrip-line-fed rectangular dielectric resonator antenna coupled with slotted ground plane for wideband circular polarization," *Microwave and Optical Technology Letters*, Vol. 58, No. 1, 206–210, 2016.
21. Pan, Y. M., K. W. Leung, and K. Lu, "Omnidirectional linearly and circularly polarized rectangular dielectric resonator antennas," *IEEE Transactions on Antennas and Propagation*, Vol. 60, No. 2, 751–759, 2011.
22. Tam, M. T. K. and R. D. Murch, "Circularly polarized circular sector dielectric resonator antenna," *IEEE Transactions on Antennas and Propagation*, Vol. 48, No. 1, 126–128, 2000.
23. Zhang, Z., X.-M. Wang, Y.-C. Jiao, and Z.-B. Weng, "Broadband circularly polarized dielectric resonator antenna with annular slot excitation," *Progress In Electromagnetics Research C*, Vol. 40, 105–117, 2013.
24. Mishra, N. K., S. Das, and D. K. Vishwakarma, "Low-profile circularly polarized cylindrical dielectric resonator antenna coupled by L-shaped resonating slot," *Microwave and Optical Technology Letters*, Vol. 59, No. 5, 996–1000, 2017.
25. Leung, K. W. and H. K. Ng, "The slot-coupled hemispherical dielectric resonator antenna with a parasitic patch: Applications to the circularly polarized antenna and wide-band antenna," *IEEE Transactions on Antennas and Propagation*, Vol. 53, No. 5, 1762–1769, 2005.